Approaches for automatic detection of mispositioning during laser welding in hidden T-joints using optical coherence tomography

Timon Ahlers[1], Ronald Pordzik[1], Thorsten Mattulat[1]
[1)] BIAS - Bremer Institut für angewandte Strahltechnik GmbH, Bremen, Germany

Abstract.
Laser welding of hidden T-joints, connecting the web-sheet through the face-sheet of the joint can provide advantages like increased lightweight potential in manufacturing sandwich structures with thin-walled cores. However, maintaining the correct positioning of the beam relative to the joint is challenging. A method to reduce the effort of positioning is using optical coherence tomography (OCT), that interferometrically measures the reflection distance inside of the keyhole during laser deep penetration welding. In this study new approaches for targeted data processing of the OCT-signal to automatically detect misalignments are presented. It is shown that considering multiple components from the inference pattern and the respective signal intensities improve the detection accuracy of misalignments.

1. Introduction

Optical coherence tomography (OCT) has become established as a robust method for geometrical measurement in the laser beam deep penetration welding process. The interferometric method provides information as a fast fourier transformed (FFT) interferometric spectrogram about how much of the reflected measurement radiation originates from a certain distance within the measurement range. Using scanners built into the processing optics, the OCT measurement spot can be flexibly positioned relative to the processing laser, so that a wide variety of in-situ optical distance measurement solutions can be implemented. Stadter et al. [1] used the technology for a leading detection of the joint position, which was used for a position control of the processing beam as well as for a geometric monitoring of the seam following the process. By coupling the measuring beam coaxially to the laser beam into the process zone, it is also possible to get geometrical information from within the keyhole. Schmoeller et al. [2] for example implemented a penetration depth control with this technology. Due to the strongly varying reflection conditions in the keyhole, targeted filtering of the measurement signal is necessary for accurate determination of the weld penetration depth. In studies such as those by Mittelstädt et al. [3] and Xie et al. [4], different approaches for statistical filtering have been investigated. These approaches use depth data, which is derived from the A-scan of the OCT sensor systems. Since no transmission of the measuring radiation occurs in metals the highest intensity of the A-scan is assumed to be induced by the reflected radiation from the actual measuring surface. All other local intensity maxima are considered as noise and are not regarded any further. Pordzik et al. [5] on the other hand have shown in their investigations that local maxima of higher orders induced through different reflection distances in the measuring range also provide relevant information for depth measurement inside the keyhole.

In a previous work by Mittelstädt et al. [6] the OCT sensor system was used for detection of misalignments in hidden T-joints. The detection of a misalignment via the OCT sensor is based on a transmission of the OCT radiation instead of a complete reflection inside a closed keyhole, as shown in Figure 1. To enable detection via a scalar threshold, the effective sample rate was derived as a measure. The effective sample rate is calculated as the percentage of measured depth values above a heuristically determined intensity threshold. This threshold is set to distinguish between valid depth data and measurement noise.

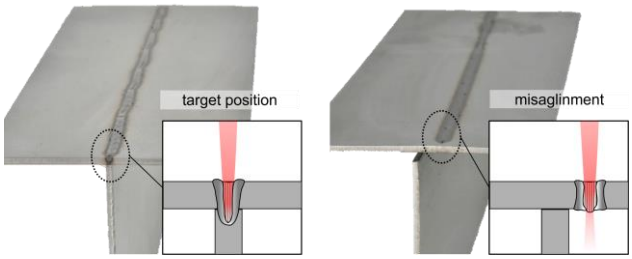

Figure 1: Different transmission conditions depending on the positioning of the process beam to the web sheet.

2. Experimental

2.1. Objective of the study

To reduce the effort of a very precise positioning of the joining zone to the laser needed for a reliable process in hidden T-joints, connecting the web-sheet through the face-sheet of the joint, by using a position control system it is first necessary to reliably detect a misalignment. In the production of genuine components, it is often not possible to implement such a sensor-based detection on the side of the web sheet. The approach developed by Mittelstädt et al. [6] allows such a detection system to be

integrated coaxial to the process beam welding through the face sheet using an industry proven OCT system for weld depth measurement. The lateral misalignment between the web sheet and laser causes that the keyhole and the surrounding weld pool are no longer centred in the web sheet. With increasing offset, the melt pool reaches the edge of the web plate and the keyhole in the web plate forms a lower opening. Mittelstädt et al. [6] showed in their investigation, that an lower opening of the keyhole causes a decrease of the reflected measurement radiation, which is indicated by the decreasing effective sample rate. In this study the potential use of further signal components as described by Pordzik et al. [5] in the A-Scan of an OCT sensor integrated in a laser beam welding optic for improved detection of misalignment in hidden T-joints was investigated.

2.2. Experimental setup

To correlate the different fractions of the OCT sensor data with the lateral offset of the laser and the web sheets welds of hidden t-joints with a defined angular offset were performed and the measurement depth as well as the intensities of the five highest peaks in the interferometric spectrogram were recorded and analysed. The measuring depth is given by the position of the local maximum in the fast Fourier transformed interferometric spectrogram [4]. The intensity describes the height of this local maximum, which is resolved in a numeric range between 1 and 999. These peaks, if significantly different from the background noise, should represent actual depth information in the measurement spot. Figure 3 illustrates different depth ranges and their representation in the intensity-depth distribution of the spectrogram. The effective sample rate, as derived by Mittelstädt et al. [6], and the intensity itself of the different peaks were considered as signals for the detection of the misalignment.

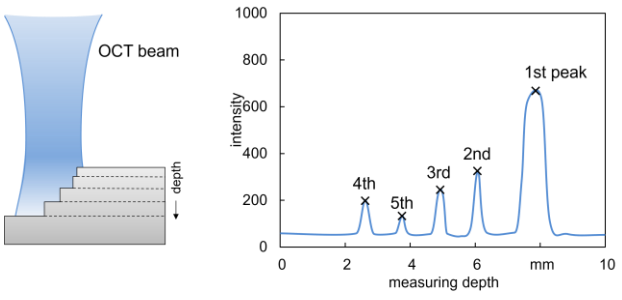

Figure 2: Schematic representation of a possible impact of different reflection distances in the measuring range into the interferometric spectrogram

The welding experiments were carried out using 2.4068 nickel as sample material. The specimens consisted of a web sheet with a thickness of 1.5 mm and a face sheet with a thickness of 0.8 mm clamped in a T-joint configuration. Both sheets were 50 mm wide and 120 mm long. For the welding experiments a Trumpf TruDisk 12002 solid state laser was used as a source of radiation. A YW52 optics from Precitec was equipped with the IDM system for OCT measurement from the same manufacturer. The measured focal diameter of the processing beam using second order moment algorithm was 306 µm (see Figure 2), while the focus position was set onto the surface of the face sheet. To enable a temporal correlation of the OCT data with a lower opening of the keyhole leaving the web sheet, a clamping device was designed in such a way that the web sheet can be monitored laterally with a highspeed camera, so that process emissions escaping from the open keyhole can be observed. A schematic of the setup can be seen in Figure 3.

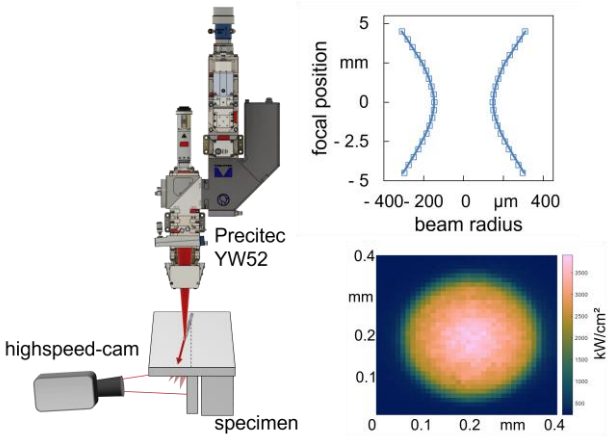

Figure 3: Schematic experimental setup (left) and caustic of the processing laser (right).

To shield the camera sensor from laser radiation a notch filter was used. A defined angular offset of the weld path to the web sheet was set. To ensure the comparability of the experiments, the repeatability of the clamping device has been examined and the lateral offset between the middle of web sheet and the laser beam was found to be below 30 µm with a standard deviation of 15 µm. To achieve a fixed keyhole position in the camera image, the laser optics and camera are operated statically, while

Table 1: System parameters of the experimental setup

processing laser	Trumpf TruDisk 12002
wavelength	1030 nm
processing optics	Precitec YW52
focal diameter	306 µm
Rayleigh length	2.297 mm
OCT system	Precitec IDM
wavelength	1.55 µm ±35 nm
power	~40 mW
measurement frequency	70 kHz
measuring range	10 mm
highspeed camera	Photron Nova S12
frame rate	10000 Hz
exposure time	10 µs

the specimen itself is moved at welding speeds of 3 m/min to 12 m/min. The laser power was adjusted from 1250 W to 4000 W to achieve an approximate welding depth of 1.6 mm using the OCT signal for estimation of the penetration depth. For the three different welding speeds two different angular offsets were applied: 2° and 4°. Each parameter set was repeated three times. Further parameters of the systems are given in Table 1.

Due to the high dynamics of the keyhole in laser beam deep penetration welding processes, the reflection conditions for the measurement radiation and consequently the OCT A-Scan varies strongly over time. To use these signals for a reliable determination of mispositioning, they initially must be filtered. The intensity signals are filtered with a floating average filter. The effective sample rate already underlies a time averaging due to its calculation over a certain amount of data points and does not require any further filtering. For the output signal to be analogous, both window sizes were kept identical. By z-normalizing the signals considered for the detection only the fluctuation of the signal is evaluated and not the absolute value, making them comparable. The z-normalization was carried out using the following formula:

$$y_{norm}(t) = \frac{(y(t)-\mu)}{\sigma}$$

The mean value μ and the standard deviation σ were calculated from corresponding signals obtained from welds without an offset. To detect a misalignment in the OCT signals a σ-surrounding was defined. If the corresponding signal deviates by more than a multiple of the standard deviation, a misalignment is detected. During data analysis, the filter window size and factor of the σ-surrounding were varied to examine their influence on the detection rate.

3. Results and discussion

For the correlation of the measured depth data with the z-normalized signals an exemplary plot obtained from a weld with an angular offset of 2° at 3 m/min is shown in Figure 4. In Figure 4a the measuring depth of the first peak is plotted. The measured depth signal can be divided into three regimes. With a small positioning error (target position), the measured depths exhibit values ranging from depths right below the specimen surface to the expected weld depth. Due to the angular offset, the positioning error increases as the process proceeds. At one point, the signal changes significantly (transition). The density of the measured values initially decreases. The data points are distributed over the entire measuring range. With increasing offset a narrow band can be observed around the target welding depth, which progressively rises to higher measuring distances. Once the positioning error became so large that the keyhole with the surrounding melt pool has completely left the web sheet, the signal becomes stationary again (misposition). In the measuring distance corresponding to the distance of the face sheet, a slight agglomeration of data points

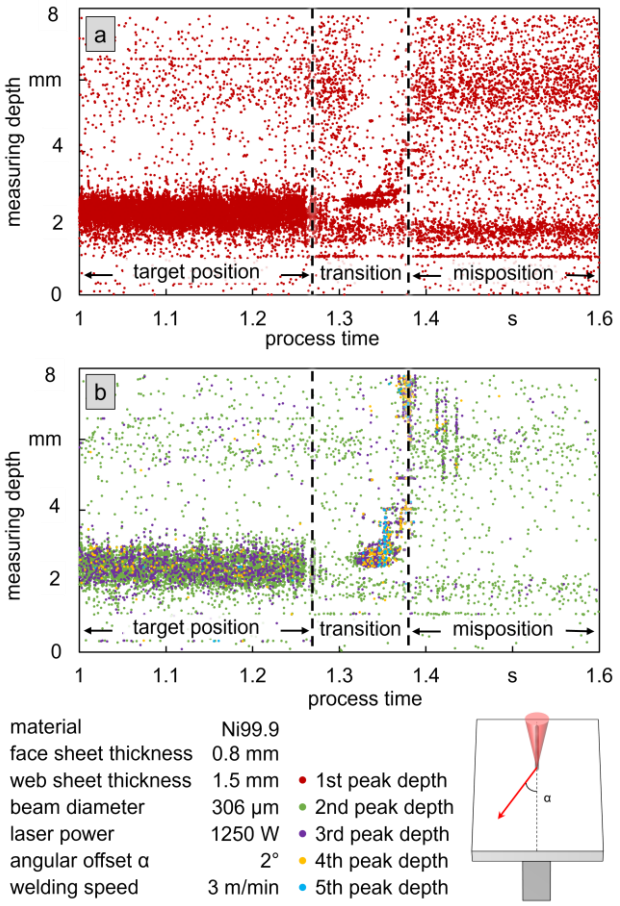

Figure 4: Exemplary plot of the a) first peak depth measurements and b) second to fifth peak depth measurements obtained from a weld with angular offset.

can be observed, even though the data point distribution is not as dense as in the signal with small positioning error. In Figure 4b results from the same weld sample are shown, but with the second to fifth order peaks instead of only the first order peak. The lower intensity peaks represent distances in the same ranges as the highest peak. Only a few measuring points scatter over the entire measuring range. An increased density of higher order measurement points can be observed in the transition regime. This is particularly noticeable for the 4th and 5th peak. Although the measurement points can be evaluated visually, a direct algorithmic decision whether there is a mispositioning is difficult to implement. Therefore, the signals require further processing. In Figure 5a the z-normalized effective sample rate of the five highest peaks is displayed for a sample with 3 m/min welding speed and an angular offset of 2°. In addition to the z-normalized signals, the time of the first lateral emission, derived from the high-speed camera image, is shown. As well as the 3σ-surrounding for each signal and the moments at which the signal trespasses these boundaries for the first time downwards and upwards. All five relative sample rates are stable before the first lateral emission apart from small fluctuations. With the first lateral emission the sample rates decrease. For the first two peaks, the sample rate drops almost immediately below -3σ. While on the third peak, it takes about

40 ms until the sample rate decreases below the threshold. In contrary, the sample rates of the fourth and fifth peak never drops below the 3σ-surrounding Following the decrease, there is an increase to be observed. For the first peak the sample rate increases only slightly above the steady level, without leaving the 3σ-surrounding. As the order of the peak increases, the relative sample rate also increases drastically. At the fifth peak the sample rate rises to about 100 σ above the average intensity. After this increase, the sample rate for the different peaks drops again. It decreases to a level comparable to the first decrease. Since the sample rate for the fifth peak in the stable process on the web sheet is very low and therefore the 3σ-surrounding is very narrow, even small fluctuations lead to a transgression of the threshold, which leads to false detections. In Figure 5b the z-normalized averaged intensity of the same sample is illustrated. The averaged intensities show almost identical signal curves as the measurement density. Individual differences are apparent in the detection. The averaged intensity at the highest peak, unlike the first order sample rate, exceeds the 3σ-surrounding during the short increase described above. The effective sample rate and the intensity signals differ slightly, which leads to different detections of misalignment in the given sample. For the first peak the averaged intensity increases in the region of the transition by more than twice the z-normalized effective sampling rate. The intensity signal of the third peak, on the other hand, decreases compared to the sampling rate by only 0.2 σ less, which already lead to no detection being possible. Since the non-detection via the intensity was caused by small numerical deviations and since the relative sample rate is a measure derived from the intensity, which entails an additional heuristically determined parameter, all further investigations were performed using the intensity.

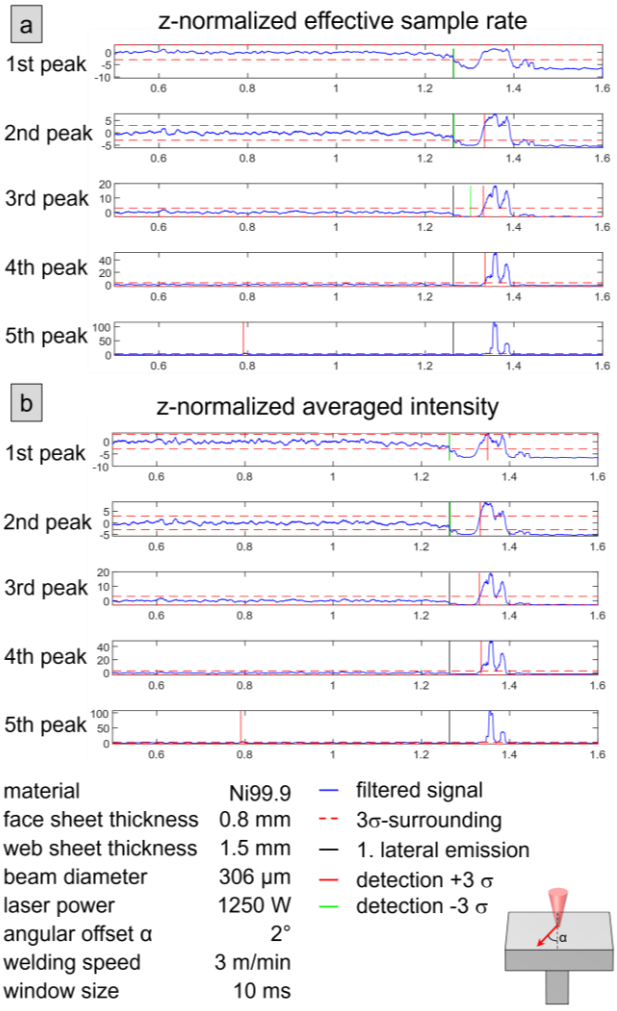

Figure 5: Signal characteristics of the five highest peaks of the z-normalized a) effective sample rate and b) averaged intensity at 3 m/min welding speed and 2° angular offset.

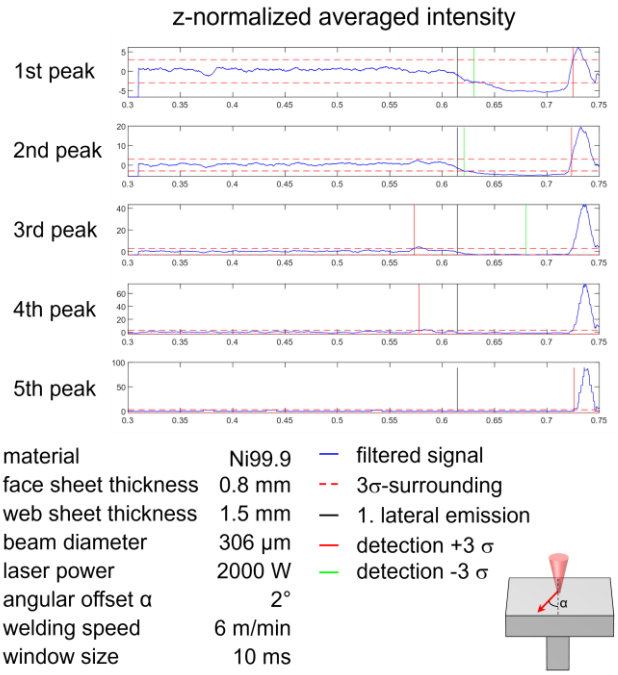

Figure 6: Z-normalized, averaged intensity of the five highest peaks in the interferometric spectrum of a sample with 6 m/min welding speed and 2° angular offset.

The characteristics of the z-normalized intensity at higher speeds is shown in Figure 6 for 6 m/min and in Figure 7 for 12 m/min. While the first decrease in the z-normalized intensity immediately after first lateral emission at 6 m/min is hardly different from that at 3 m/min, for 12 m/min no decrease in the intensity is observed within the ordinary variation of the signal. The short increase in intensity is significantly greater at 6 m/min for the first to fourth peak. For the fifth peak, the intensity rises in the transition regime to the same level compared to the sample at 3 m/min. For the 12 m/min sample, however, the short increase of the z-normalized intensity decreases compared to the 3 m/min sample, the intensity of the first peak does not leave the 3σ-surrounding. At the fourth and fifth peak, on the other hand, false detections occur, before the first lateral emission. The time interval between the first lateral emission and said increase in intensity shows no direct correlation to the welding speed. At 3 m/min welding speed it takes on average 70 ms ± 9 ms after first lateral emission to leave the 3σ-surrounding upwards, this increases to 108 ms ± 4 ms for 6 m/min. At 12 m/min, however, the

duration decreases again to 89 ms. Here, the variance of 36 ms is significantly higher.

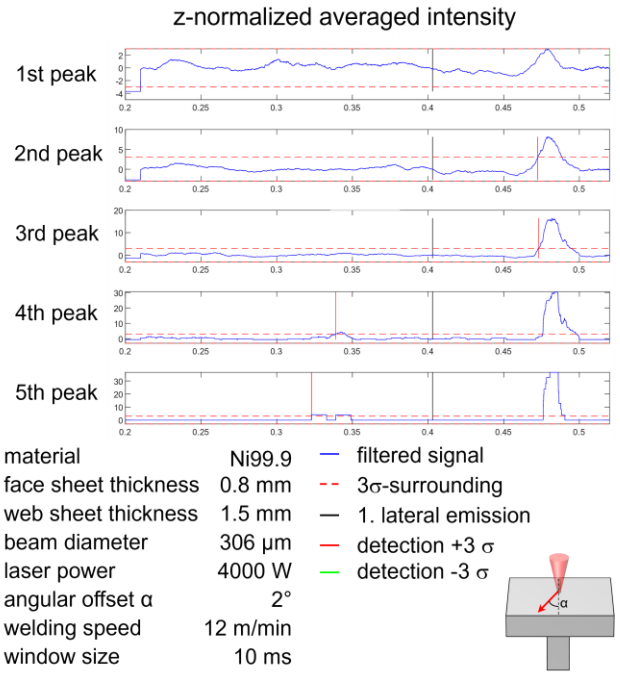

Figure 7: Z-normalized, averaged intensity of the five highest peaks in the interferometric spectrum of a sample with 12 m/min welding speed and 2° angular offset

An overview of a possible detection of misalignment via peaks of different orders is shown in Figure 8. The table illustrates the detection depending on the welding speed and the considered peak. All Samples with 2° angular offset were evaluated, while the floating average filter size was 10 ms and a 3σ-surrounding was used for thresholding. Using the intensity of the first peak and the given detection parameters the mispositioning in all samples with welding speeds of 3 m/min and 6 m/min could be detected. To be able to detect the mispositioning at 12 m/min, the intensity of peak 2 or 3 must be considered. Due to the narrow 3σ-surrounding, the higher order peaks are prone to raise false detections before the first lateral emission detected via the highspeed imaging. At 6 m/min, one specimen resulted in false detection at the third and fourth peak, while the fifth peak again did not trigger until the transition regime. Due to the high variation of the signal at high welding speeds, the fluctuation in the intensity of the highest peaks caused by leaving the web sheet is relatively small, so that detection via the given σ-surrounding is no longer possible. The increase of the intensity in the transition regime in the 2nd and 3rd peaks, on the other hand, is so prominent that the mispositioning can still be detected. The number of measurement points decreases significantly with increasing peak order, resulting in small standard deviations of the averaged intensities for higher order peaks, which consequently leads to higher sensitivity for false detections, when short-term fluctuations cause the intensities for these peaks to increase. A crucial aspect in the selection of the signal, however, is the detection time. While the first decrease in intensity takes place within a few milliseconds, the detection of the following increase takes over 100 ms. Even at low welding velocities of 3 m/min, this results in a welded distance of 5 mm before any reaction is possible. Therefore, the highest peak with the most prominent first decrease in intensity remains critical for fast detection at low speeds.

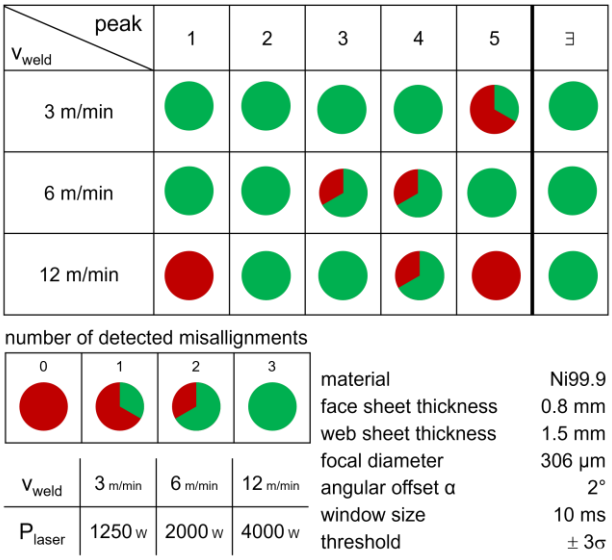

Figure 8: Detection of misalignment via the different peaks at varying speeds for 2°angular offset with a window width of the averaging filter of 10 ms and a threshold of ± 3σ.

The detection rate over all examined welding speeds and angular offsets with variation of the detection parameters is shown in Figure 9. The influence of the window width of the floating average filter on the detection rate for different combinations of logically linked intensity signals is shown in Figure 9a. If only the intensity of the highest peak is used for detection, the detection rate increases with smaller window widths. With a window width of 2.5 ms, 77.78% of the samples could be detected properly. The same trend can be observed when using first and second peak in combination. By triggering when one of the two signals leaves the corresponding 3σ-surrounding, mispositioning can be correctly detected in up to 94.44% of the samples examined. For the combination of the second and third peak the same detection rate was achieved for window sizes from 2.5 ms to 10 ms. An opposite trend can be observed for combinations of higher order peak intensities. Here the detection rate increases with the window width. By combining all five examined intensity signals, a detection rate above 94.44% could be achieved for all examined window sizes. For 5 ms filter window size all samples were detected correctly. In Figure 9b the detection rates at 10 ms filter window size for different thresholds are shown. For the first peak intensity signal, the σ-surroundings studied show no influence on the detection rate. Except for the combination of the 4th and 5th peaks, the detection rate at 3σ is higher or the same as at 4σ. For all combinations the detection rate achieved with 3.5σ was lower than 3σ or 4σ. When varying the detection parameters, no clear trends are evident regarding the detection rate.

Although all misalignments could be correctly detected in one parameter set by the appropriate combination of different peaks, it is still necessary to check which intensity signals are suitable for each application. The parameters must be optimized heuristically for each case.

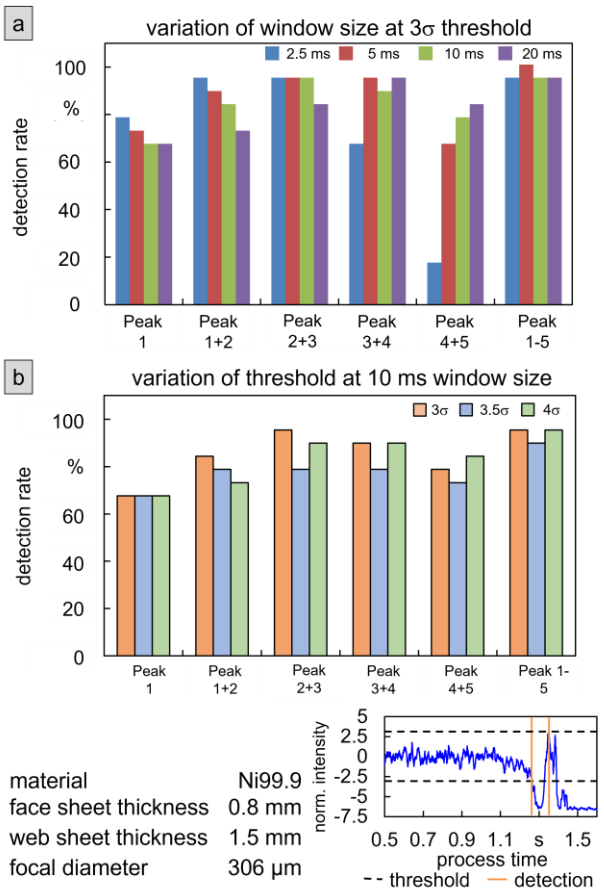

Figure 9: Detection rate for varied a) floating average filter window size and b) thresholds of the σ-surrounding.

Conclusion

The averaged intensity gives a qualitative equivalent indication of the mispositioning of the web sheet in a hidden T-joint compared to the effective sample rate and at the same time eliminates a heuristic parameter. Using not only the intensity of the highest peak but also intensities of the higher order peaks the rate of correct detection of mispositioning increased in the samples studied. This applies in particular to higher welding speeds, where reliable detection via the highest peak is no longer possible. To use the increase in the transition regime for detection however causes higher detection delays.

Acknowlegements

The project on which this publication is based was funded by the German Federal Ministry of Education and Research under grant number 03HY119F.The responsibility for the contents of the publication lies with the authors.

Bundesministerium für Bildung und Forschung

Contact details

BIAS – Bremer Institut für angewandte Strahltechnik GmbH

Klagenfurter Str.5, 28359 Bremen

M.Sc. Timon Ahlers

ahlers@bias.de

References

[1] Stadter, Christian; Schmoeller, Maximilian; Zeitler, Martin; Tueretkan, Volkan, Munzert, Ulrich, Zaeh, Michael F. (2019): Process control and quality assurance in remote laser beam welding by optical coherence tomography, Journal of Laser Applications, 2019, 31, p. 022408.

[2] Schmoeller, Maximilian; Weiss, Tony; Goetz, Korbinian; Stadter, Christian; Bernauer, Christian; Zaeh, Michael F. (2022): Inline Weld Depth Evaluation and Control Based on OCT Keyhole Depth Measurement and Fuzzy Control, Processes 10, p. 1422

[3] Mittelstädt, Christoph; Mattulat, Thorsten; Seefeld, Thomas; Kogel-Hollacher, Markus (2019): Novel approach for weld depth determination using optical coherence tomography measurement in laser deep penetration welding of aluminum and steel, Journal of Laser Applications, 2019, 31, p. 022007.

[4] Xie, Guanming; Wang, Sanhong; Zhang, Yueqiang; Hu, Biao; Fu ,Yu; Yu, Qifeng; Li, You (2023): An Efficient Method for Laser Welding Depth Determination Using Optical Coherence Tomography, Sensors, 2023, 23, p. 5223.

[5] Pordzik, Ronald; Ahlers, Timon; Mattulat, Thorsten (2023): Enhancement of weld depth analysis in laser welding by extension of the oct data scope, Lasers in Manufacturing Conference 2023, Proceedings, 2023.

[6] Mittelstädt, Christoph; Seefeld, Thomas; Vollertsen, Frank (2019): Laser blank-rim melting for robust laser welding of hidden T-joints with OCT-based position control, Lasers in Manufacturing Conference 2019, Proceedings, 2019.